Geophysical Journal International

Geophys. J. Int. (2016) **206,** 1718–1729
Advance Access publication 2016 June 24
GJI Marine geosciences and applied geophysics

doi: 10.1093/gji/ggw237

Contraction pre-conditioner in finite-difference electromagnetic modelling

Nikolay Yavich[1] and Michael S. Zhdanov[1,2,3]

[1] *Moscow Institute of Physics and Technology, Moscow, Russia. E-mail: nbyavich@gmail.com*
[2] *University of Utah, Salt Lake City, UT, USA*
[3] *TechnoImaging, Salt Lake City, UT, USA*

Accepted 2016 June 21. Received 2016 June 18; in original form 2015 November 11

SUMMARY

This paper introduces a novel approach to constructing an effective pre-conditioner for finite-difference (FD) electromagnetic modelling in geophysical applications. This approach is based on introducing an FD contraction operator, similar to one developed for integral equation formulation of Maxwell's equation. The properties of the FD contraction operator were established using an FD analogue of the energy equality for the anomalous electromagnetic field. A new pre-conditioner uses a discrete Green's function of a 1-D layered background conductivity. We also developed the formulae for an estimation of the condition number of the system of FD equations pre-conditioned with the introduced FD contraction operator. Based on this estimation, we have established that the condition number is bounded by the maximum conductivity contrast between the background conductivity and actual conductivity. When there are both resistive and conductive anomalies relative to the background, the new pre-conditioner is advantageous over using the 1-D discrete Green's function directly. In our numerical experiments with both resistive and conductive anomalies, for a land geoelectrical model with 1:10 contrast, the method accelerates convergence of an iterative method (BiCGStab) by factors of 2–2.5, and in a marine example with 1:50 contrast, by a factor of 4.6, compared to direct use of the discrete 1-D Green's function as a pre-conditioner.

Key words: Numerical solutions; Numerical approximations and analysis; Electromagnetic theory; Magnetotellurics; Marine electromagnetics.

1 INTRODUCTION

Interpretation of electromagnetic (EM) geophysical data as well as EM survey design require an efficient forward modelling method. There are several major techniques of 3-D EM modelling which have found wide applications in geophysics—integral equations (IE; e.g. Dmitriev 1969; Hohmann 1975; Weidelt 1975; Newman *et al.* 1986; Hursan & Zhdanov 2002), finite difference (FD; e.g. Yee 1966; Druskin & Knizhnerman 1994; Mackie *et al.* 1994; Weiss & Newman 2002; Weiss & Constable 2006; Maaø 2007) and finite element methods (e.g. Marinenko *et al.* 2009; Cai *et al.* 2014; Koldan *et al.* 2014). Each of these methods has its own advantages and disadvantages (Avdeev 2005; Zhdanov 2009). There are several principal differences and related advantages and disadvantages between the IE and FD methods. For example, the system of FD equations has a sparse matrix, while the system of IE equations is described by a full matrix. The standard IE approach is usually based on the uniform grid in the horizontal directions, while the FD method can use arbitrary stretched discretization grids. There are quite a few other fundamental differences, which were analysed in depth in literature. In this paper we discuss the finite-difference approach, as it combines simple implementation and flexibility.

The most time-consuming step in FD modelling is the solution of the corresponding system of linear equations. This system is sparse, complex and generally quite large. Beyond that, the system is very ill conditioned due to the large ratio of the size of the computational domain to the smallest grid step (Druskin & Knizhnerman 1994) and to the presence of a highly resistive air layer. The use of upward continuation procedure allows elimination of the resistive air layer (Weidelt 2000; Commer & Newman 2004) and subsequent improvement of the system matrix condition number. However, the procedure is difficult to implement when the earth's surface has any topographic features.

The choice of an efficient method of solving the linear system of FD equations is crucial in order to minimize the execution time of forward modelling algorithms. This is especially important for EM inversion requiring sequential solution of multiple forward problems. Recently, significant advances have been made in developing the direct solvers for forward EM problems (e.g. Streich 2009; da Silva *et al.* 2012; Grayver *et al.* 2013; Jaysaval *et al.* 2014). However, the direct solvers still impose challenging memory requirements for large-scale 3-D problems, which makes the iterative solvers more attractive in geophysical applications (Saad 2003).

The performance of an iterative solver is essentially dictated by its pre-conditioners. A diagonal or Jacobi pre-conditioner may be used (see, e.g. Newman & Alumbaugh 2002; Cai *et al.* 2014). However, its performance degrades after a few tens of iterations. More efficient pre-conditioners have been developed based, for example, on explicit enforcement of the charge conservation law (Smith 1996), or on sequential relaxation in a hierarchy of computational grids (i.e. multigrid; Arnold *et al.* 2000; Mulder 2008, 2007; Yavich & Scholl 2012) or on incomplete factorization, (i.e. ILU; Um *et al.* 2013; Grayver & Bürg 2014; Puzyrev & Cela 2015) or on domain decomposition methods (Ren *et al.* 2014). Zaslavsky *et al.* (2011) introduced a pre-conditioner based on the FD Green's functions computed for the horizontally layered background model. That approach was shown to be practical for a variety of large complex problems. Zaslavsky *et al.* (2011) also demonstrated that Green's function based pre-conditioner was efficient, memory-economical, and an improvement over those now used in practice (e.g. a sparse direct solver).

In the work by Singer (1995), Zhdanov & Fang (1997), Hursan & Zhdanov (2002), Zhdanov (2002), Singer *et al.* (2003) and Singer (2008), a novel approach to constructing a pre-conditioner for the IE method was introduced based on a specially chosen contraction operator (CO). This approach takes into account the physical nature of the system of IE equations and uses the pre-conditioner based on the energy inequality for the anomalous EM field (Pankratov *et al.* 1995). This inequality represents the fundamental physical fact that the energy flow of the anomalous EM field outside the domain with anomalous conductivity is always non-negative. The goal of our paper is to demonstrate that the idea of using the CO, successfully developed for the IE method, could be applied to the FD solutions as well. At the same time we keep all the benefits that FD provides over IE. For example, efficient modelling on non-uniform computational grids, accommodation of complex geometries, as well as semi-infinite and infinite bodies.

We introduce a finite-difference analogue of the IE CO. The FD CO is then used to develop a new pre-conditioner for effective FD modelling. We also analyse the condition number in order to determine for which models a contraction pre-conditioner is more beneficial than the conventional Green's functions pre-conditioner. We illustrate the performance of the developed approach with numerical examples including 3-D land magnetotelluric (MT) and marine controlled-source EM modelling.

2 DIFFERENTIAL FORMULATION OF AN ELECTROMAGNETIC FORWARD MODELLING PROBLEM AND ENERGY EQUALITY

We begin with a short summary of the basic differential equations used in an EM forward modelling problem and their finite difference approximation. The electrical conductivity of the geoelectrical model in a general case is a real-valued, positive function of spatial variables, $\sigma = \sigma(x, y, z)$. In a general case, the conductivity is assumed to be non-zero in the air. The electric field, $\boldsymbol{E} = \boldsymbol{E}(x, y, z)$, satisfies the following second order differential equation:

$$\text{curl curl } \boldsymbol{E} - i\omega\mu_0\sigma\boldsymbol{E} = i\omega\mu_0\boldsymbol{J}, \tag{1}$$

where $\boldsymbol{J} = \boldsymbol{J}(x, y, z)$ is a known current density in the source, i is the complex unity, ω is the angular frequency and μ_0 is the magnetic permeability of the vacuum. This equation is completed with the corresponding boundary conditions at infinity (Zhdanov 2009).

The magnetic field, $\boldsymbol{H} = \boldsymbol{H}(x, y, z)$, can be determined using Faraday's law,

$$\boldsymbol{H} = \frac{1}{i\omega\mu_0}\text{curl } \boldsymbol{E}. \tag{2}$$

Following the conventional approach to EM forward modelling, which allows us to avoid a singularity in the source (Zhdanov 2009), we assume that the total conductivity is a superposition of the background and anomalous parts, $\sigma(x, y, z) = \sigma_b(x, y, z) + \sigma_a(x, y, z)$, and we represent the electric and magnetic fields as a sum of the background and anomalous components, respectively:

$$\begin{aligned}\boldsymbol{E}(x, y, z) &= \boldsymbol{E}_b(x, y, z) + \boldsymbol{E}_a(x, y, z),\\ \boldsymbol{H}(x, y, z) &= \boldsymbol{H}_b(x, y, z) + \boldsymbol{H}_a(x, y, z),\end{aligned} \tag{3}$$

where $\sigma_a(x, y, z)$ is non-zero within an anomalous domain only. We call the anomalous domain the volume(s), D, where $\sigma(x, y, z)$ differs from $\sigma_b(x, y, z)$. The anomalous domain may not be bounded or connected. The background and anomalous electric fields satisfy the following equations:

$$\text{curl curl } \boldsymbol{E}_b - i\omega\mu_0\sigma_b\boldsymbol{E}_b = i\omega\mu_0\boldsymbol{J}, \tag{4}$$

$$\text{curl curl } \boldsymbol{E}_a - i\omega\mu_0\sigma_b\boldsymbol{E}_a = i\omega\mu_0\boldsymbol{J}_a, \tag{5}$$

where $\boldsymbol{J}_a = \sigma_a(\boldsymbol{E}_a + \boldsymbol{E}_b)$ is the density of the excess electric current within the domain with anomalous conductivity. The advantage of this approach is that we can use the known solutions for the background field and solve the differential equations for the anomalous field only. For example, in a case where the horizontally layered background model is excited by an electric or magnetic dipole, the background electric field could be found explicitly using the Hankel transform (Zhdanov 2009). We thus will assume that the background model is invariant to the horizontal coordinates, $\sigma_b(x, y, z) \equiv \sigma_b(z)$.

The differential equations (5) are solved in a bounded rectangular hexahedral computational domain V and completed with zero Dirichlet boundary condition on its boundary S,

$$\boldsymbol{E}_a \times \boldsymbol{\nu} = 0, \tag{6}$$

where $\boldsymbol{\nu}$ is the unit outward normal for S.

Interestingly, the energy inequality (Pankratov *et al.* 1995; Zhdanov & Fang 1997) takes the form of an equality for the systems (5) and (6) and under the introduced assumption that the conductivity is real-valued. Let us derive this equality as it will play an important role in the discussion later. Scalar multiplication of eq. (5) by $\boldsymbol{E}_a^*$ and integration over V gives us the following equation:

$$\begin{aligned}&\int_V \boldsymbol{E}_a^* \cdot \text{curl curl } \boldsymbol{E}_a \mathrm{d}V - i\omega\mu_0 \int_V \sigma_b \boldsymbol{E}_a^* \cdot \boldsymbol{E}_a \mathrm{d}V\\ &= i\omega\mu_0 \int_V \boldsymbol{E}_a^* \cdot \boldsymbol{J}_a \mathrm{d}V.\end{aligned} \tag{7}$$

The following integral identity is known (see, e.g. Van Bladel 2007) to hold for any two vector-functions, $\boldsymbol{F}$ and $\boldsymbol{G}$,

$$\int_V \boldsymbol{F} \cdot \text{curl } \boldsymbol{G} \mathrm{d}V = \int_V \boldsymbol{G} \cdot \text{curl } \boldsymbol{F} \mathrm{d}V + \int_S \boldsymbol{F} \cdot (\boldsymbol{\nu} \times \boldsymbol{G}) \mathrm{d}S. \tag{8}$$

Applying it to the first term of eq. (7), we receive:

$$\begin{aligned}&\int_V |\text{curl } \boldsymbol{E}_a|^2 \, \mathrm{d}V + \int_S \boldsymbol{E}_a^* \cdot (\boldsymbol{\nu} \times \text{curl } \boldsymbol{E}_a) \mathrm{d}S\\ &- i\omega\mu_0 \int_V \sigma_b \, |\boldsymbol{E}_a|^2 \, \mathrm{d}V = i\omega\mu_0 \int_V \boldsymbol{E}_a^* \cdot \boldsymbol{J}_a \mathrm{d}V.\end{aligned} \tag{9}$$

The integrand of the surface integral is equivalent to [curl $\boldsymbol{E}_a \cdot (\boldsymbol{E}_a^* \times \boldsymbol{\nu})$]. This expression is zero due to eq. (6) and consequently the surface integral vanishes,

$$\int_V |\text{curl } \boldsymbol{E}_a|^2 \, \mathrm{d}V - i\omega\mu_0 \int_V \sigma_b \, |\boldsymbol{E}_a|^2 \, \mathrm{d}V = i\omega\mu_0 \int_{V\cap D} \boldsymbol{E}_a^* \cdot \boldsymbol{J}_a \mathrm{d}V. \tag{10}$$

where we have reduced the volume integration in the right-hand side to the intersection of domains D and V, because excess electric current, $\boldsymbol{J}_a$, vanishes outside the anomalous domain D. By dividing by $i\omega\mu_0$ and taking the real part, we finally arrive at the following energy equality:

$$\int_V \sigma_b \, |\boldsymbol{E}_a|^2 \, \mathrm{d}V + \text{Re} \int_{V\cap D} \boldsymbol{E}_a^* \cdot \boldsymbol{J}_a \mathrm{d}V = 0. \tag{11}$$

It states that all the energy emitted by the excess electric current within the domain with anomalous conductivity is converted into Joule heating within the computational domain. This result is justified because eq. (6) states that there is no electric field propagation outside the domain of computations, V. In Appendix B, we have proved that the FD approximations of the anomalous electric field and current satisfy a discrete energy equality.

3 LINEAR SYSTEMS OF FINITE-DIFFERENCE EQUATIONS AND THE CORRESPONDING PRE-CONDITIONERS

Differential equations (1) or (5) for total or anomalous electric fields can be transformed into the systems of algebraic equations using the finite-difference discretization (e.g. Yee 1966; Druskin & Knizhnerman 1994; Mackie *et al.* 1994; Weiss & Newman 2002; Weiss & Constable 2006). For completeness, the details of this discretization on a staggered grid are given in Appendix A. The linear system of algebraic equations corresponding to differential eq. (1) has the following form:

$$\boldsymbol{A}\boldsymbol{e} = i\omega\mu_0 \boldsymbol{j}, \tag{12}$$

where vector $\boldsymbol{e} \in \mathbb{C}^n$ is the discrete total electric field and $\boldsymbol{j} \in \mathbb{C}^n$ is the discrete current density, and n is defined in eq. (A7).

The system matrix $\boldsymbol{A}$ is complex, square, sparse, non-singular and has at most 13 non-zero entries per row. The system matrix inherits some properties of the differential operator involved in (1). In particular, the matrix admits the following splitting:

$$\boldsymbol{A} = \boldsymbol{R} - i\omega\mu_0 \boldsymbol{\Sigma}, \tag{13}$$

where $\boldsymbol{R}$ is a real-valued matrix corresponding to FD discretization of the curl-curl operator, $\boldsymbol{\Sigma}$ is a diagonal real positive-definite matrix with its diagonal values equal to the edge-sampled conductivities $\sigma(x, y, z)$ (A5).

Following the way we decomposed the total conductivity and EM fields into their background and anomalous parts in the previous section, we introduce a finite-difference approximation of eq. (4):

$$\boldsymbol{A}_b \boldsymbol{e}_b = i\omega\mu_0 \boldsymbol{j}, \tag{14}$$

where $\boldsymbol{e}_b$ is a vector of the discrete background electric field on the staggered grid, $\boldsymbol{A}_b$ is the system matrix corresponding to the operator of eq. (4),

$$\boldsymbol{A}_b = \boldsymbol{R} - i\omega\mu_0 \boldsymbol{\Sigma}_b, \tag{15}$$

and $\boldsymbol{\Sigma}_b$ is a diagonal matrix with edge-sampled background conductivity, σ_b. We can also define discretized anomalous conductivity, $\boldsymbol{\Sigma}_a$, which is related with $\boldsymbol{\Sigma}$ and $\boldsymbol{\Sigma}_b$ as follows: $\boldsymbol{\Sigma} = \boldsymbol{\Sigma}_b + \boldsymbol{\Sigma}_a$. Obviously, the finite-difference approximation of eq. (5) for the anomalous electric field, $\boldsymbol{e}_a$, takes the following form:

$$\boldsymbol{A}_b \boldsymbol{e}_a = i\omega\mu_0 \boldsymbol{j}_a, \tag{16}$$

where $\boldsymbol{j}_a$ is a vector of discrete excess electric current:

$$\boldsymbol{j}_a = \boldsymbol{\Sigma}_a (\boldsymbol{e}_a + \boldsymbol{e}_b). \tag{17}$$

As it was discussed in the Introduction, the most effective way of solving the matrix equations (12) and (16) for large-scale problems is based on iterative methods and the use of the corresponding pre-conditioners. There are many different methods of introducing pre-conditioners for a general matrix equation. The most general expression for a pre-conditioned matrix eq. (12) can be written as follows:

$$\boldsymbol{M}_1 \boldsymbol{A} \boldsymbol{M}_2 \left(\boldsymbol{M}_2^{-1} \boldsymbol{e}\right) = i\omega\mu_0 \boldsymbol{M}_1 \boldsymbol{j}, \tag{18}$$

where $\boldsymbol{M}_1$ and $\boldsymbol{M}_2$ are the left and right pre-conditioners, respectively.

Formula (18) can be presented in an equivalent way as follows,

$$\tilde{\boldsymbol{A}} \tilde{\boldsymbol{e}} = i\omega\mu_0 \tilde{\boldsymbol{j}}, \tag{19}$$

where $\tilde{\boldsymbol{A}} = \boldsymbol{M}_1 \boldsymbol{A} \boldsymbol{M}_2$, $\tilde{\boldsymbol{e}} = \boldsymbol{M}_2^{-1} \boldsymbol{e}$, $\tilde{\boldsymbol{j}} = \boldsymbol{M}_1 \boldsymbol{j}$. The pre-conditioners are usually selected in such a way that matrix $\tilde{\boldsymbol{A}} = \boldsymbol{M}_1 \boldsymbol{A} \boldsymbol{M}_2$ is better conditioned than $\boldsymbol{A}$, which ensures a better convergence of the applied iterative method.

In many cases, one can use the left pre-conditioner only, assuming that $\boldsymbol{M}_2 = \boldsymbol{I}$, where $\boldsymbol{I}$ is the identity matrix. For example, Zaslavsky *et al.* (2011) suggested using a volume integral equation approach to arrive at an effective pre-conditioning operator for the FD solver for the magnetic field. In our formulation, this pre-conditioner can be formally defined as $\boldsymbol{M}_1 = \boldsymbol{A}_b^{-1}$, where $\boldsymbol{A}_b$ is the system matrix defined in eq. (15). Thus, the pre-conditioned system of equations takes the following form:

$$\tilde{\boldsymbol{A}}' e = i\omega\mu_0 \tilde{\boldsymbol{j}}', \tag{20}$$

where $\tilde{\boldsymbol{A}}' = \boldsymbol{A}_b^{-1} \boldsymbol{A}$ and $\tilde{\boldsymbol{j}}' = \boldsymbol{A}_b^{-1} \boldsymbol{j}$.

The pre-conditioned eq. (16) for the anomalous field can be written as follows:

$$\boldsymbol{e}_a = i\omega\mu_0 \boldsymbol{A}_b^{-1} \boldsymbol{\Sigma}_a (\boldsymbol{e}_a + \boldsymbol{e}_b). \tag{21}$$

We can introduce a discrete Green's operator for the background media, $\boldsymbol{\mathcal{G}}_b$,

$$\boldsymbol{\mathcal{G}}_b = i\omega\mu_0 \boldsymbol{A}_b^{-1}, \tag{22}$$

and write the pre-conditioned eq. (21) as follows:

$$\boldsymbol{e}_a = \boldsymbol{\mathcal{G}}_b \, \boldsymbol{\Sigma}_a \, (\boldsymbol{e}_a + \boldsymbol{e}_b). \tag{23}$$

Thus, we can see that computing the pre-conditioner based on the background model is equivalent to the calculation of the discrete Green's operator. This approach is especially efficient in the case of a layered background conductivity model, because there is a technique available for inverting $\boldsymbol{A}_b$ via discrete separation of variables (Martikainen *et al.* 2003; Zaslavsky *et al.* 2011). The arithmetical complexity to compute $\boldsymbol{A}_b^{-1} \boldsymbol{u}$ for arbitrary $\boldsymbol{u} \in \mathbb{C}^n$ on a non-uniform grid is $O(N_x N_y N_z (N_x + N_y))$, and the auxiliary memory needed is $O(n)$. Under the assumption that N_x,N_y and N_z are of the same order, the complexity is equal to $O(n^{4/3})$ due to (A7).

The multiplication by the FD Green's function, required for computing the pre-conditioner described by eq. (23) involves the following key steps: (1) diagonal scaling to symmetrize the equation matrix; (2) 2-D forward discrete Fourier transform of $\boldsymbol{E}_x$, $\boldsymbol{E}_y$ and $\boldsymbol{E}_z$ within each grid layer; (3) find the corresponding spectra by solving seven- and tridiagonal systems (4) 2-D inverse Fourier transform of the spectra; and (5) removing the impact of diagonal scaling. The interested reader is referred to the papers mentioned above for technical details.

Let us estimate the condition number of the pre-conditioned system (20). Assume that the following double inequality holds:

$$\alpha\sigma_b(z) \le \sigma(x, y, z) \le \beta\sigma_b(z), \quad 0 < \alpha \le 1 \le \beta, \quad (x, y, z) \in V. \tag{24}$$

This inequality means that the anomalous domains are neither perfect conductors nor insulators. With the help of eq. (A5), an analogous inequality for the coefficient matrices can be derived:

$$\alpha\boldsymbol{\Sigma}_b \le \boldsymbol{\Sigma} \le \beta\boldsymbol{\Sigma}_b. \tag{25}$$

Let us introduce a pseudo-scalar product in the complex linear space $\mathbb{C}^n$:

$$\begin{aligned}(\boldsymbol{u}, \boldsymbol{v}) = &\sum u_{i+\frac{1}{2}\,j\,k} v_{i+\frac{1}{2}\,j\,k} |V_{i+\frac{1}{2}\,j\,k}| \\ &+ \sum u_{i\,j+\frac{1}{2}\,k} v_{i\,j+\frac{1}{2}\,k} |V_{i\,j+\frac{1}{2}\,k}| \\ &+ \sum u_{i\,j\,k+\frac{1}{2}} v_{i\,j\,k+\frac{1}{2}} |V_{i\,j\,k+\frac{1}{2}}|.\end{aligned} \tag{26}$$

Here, the first sum involves the discrete entries of u_x and v_x as well as the volume around the respective internal x edge. Similarly, the second sum involves discrete u_y and v_y, the third involves u_z and v_z (see eqs A3 and A4, for notations). This expression does not form a conventional scalar product; however, a vector norm in $\mathbb{C}^n$ could be defined as follows:

$$\|\boldsymbol{u}\|^2 = (\boldsymbol{u}^*, \boldsymbol{u}), \tag{27}$$

where the complex conjugation is marked by an asterisk *.

We note that matrices $\boldsymbol{A}$ and $\boldsymbol{R}$ are symmetric under the introduced pseudo-scalar product,

$$(\boldsymbol{Au}, \boldsymbol{v}) = (\boldsymbol{u}, \boldsymbol{Av}), \quad (\boldsymbol{Ru}, \boldsymbol{v}) = (\boldsymbol{u}, \boldsymbol{Rv}), \quad \forall\, \boldsymbol{u}, \boldsymbol{v} \in \mathbb{C}^n. \tag{28}$$

Moreover, $\boldsymbol{R}$ is a semi-positive definite matrix,

$$(\boldsymbol{u}^*, \boldsymbol{Ru}) \ge 0, \tag{29}$$

These properties of the applied discretization are well known (see, e.g. Schuhmann & Weiland 2001) and will be used extensively below.

Using this pseudo-scalar product and eqs (13), (24) and (25), we can write the following:

$$\begin{aligned}|(\boldsymbol{u}^*, \boldsymbol{Au})| &= \sqrt{(\boldsymbol{u}^*, \boldsymbol{Ru})^2 + (\boldsymbol{u}^*, \omega\mu_0\boldsymbol{\Sigma u})^2} \\ &\le \sqrt{(\boldsymbol{u}^*, \beta\boldsymbol{Ru})^2 + (\boldsymbol{u}^*, \beta\omega\mu_0\boldsymbol{\Sigma}_b\boldsymbol{u})^2} \\ &= \beta\sqrt{(\boldsymbol{u}^*, \boldsymbol{Ru})^2 + (\boldsymbol{u}^*, \omega\mu_0\boldsymbol{\Sigma}_b\boldsymbol{u})^2} \\ &= \beta|(\boldsymbol{u}^*, \boldsymbol{A}_b\boldsymbol{u})|.\end{aligned} \tag{30}$$

Similarly,

$$|(\boldsymbol{u}^*, \boldsymbol{Au})| \ge \alpha|(\boldsymbol{u}^*, \boldsymbol{A}_b\boldsymbol{u})|. \tag{31}$$

These relations allow us to estimate the condition number of the pre-conditioned system $\boldsymbol{A}_b^{-1}\boldsymbol{A}$.

In a case of a system with Hermitian positive-definite matrix $\boldsymbol{M}$ with a left pre-conditioner $\boldsymbol{Q}$ having the same properties, the pre-conditioner-related inner product can be introduced:

$$(\boldsymbol{u}^*, \boldsymbol{v})_Q = (\boldsymbol{u}^*, \boldsymbol{Qv}), \tag{32}$$

and the condition number can be estimated as follows (Lemma 2.4.1 and Theorem 2.5.1, Quarteroni & Valli 2008),

$$\operatorname{cond} \boldsymbol{Q}^{-1}\boldsymbol{M} = \frac{\max\limits_{u\ne0} \dfrac{(\boldsymbol{u}^*, \boldsymbol{Q}^{-1}\boldsymbol{Mu})_Q}{(\boldsymbol{u}^*, \boldsymbol{u})_Q}}{\min\limits_{u\ne0} \dfrac{(\boldsymbol{u}^*, \boldsymbol{Q}^{-1}\boldsymbol{Mu})_Q}{(\boldsymbol{u}^*, \boldsymbol{u})_Q}} = \frac{\max\limits_{u\ne0} \dfrac{(\boldsymbol{u}^*, \boldsymbol{Mu})}{(\boldsymbol{u}^*, \boldsymbol{Qu})}}{\min\limits_{u\ne0} \dfrac{(\boldsymbol{u}^*, \boldsymbol{Mu})}{(\boldsymbol{u}^*, \boldsymbol{Qu})}}. \tag{33}$$

In our case, unfortunately, matrices $\boldsymbol{A}$ and $\boldsymbol{A}_b$ are not Hermitian and are not even normal (they do not commute with their adjoint matrices). Consequently, the above argument is not applicable. Heuristically, we use the latter fraction to approximate the condition number. Combining it with eqs (30) and (31), we obtain the following estimate for the condition number:

$$\operatorname{cond} \boldsymbol{A}_b^{-1}\boldsymbol{A} \approx \frac{\max\limits_{u\ne0} \left|\dfrac{(\boldsymbol{u}^*, \boldsymbol{Au})}{(\boldsymbol{u}^*, \boldsymbol{A}_b\boldsymbol{u})}\right|}{\min\limits_{u\ne0} \left|\dfrac{(\boldsymbol{u}^*, \boldsymbol{Au})}{(\boldsymbol{u}^*, \boldsymbol{A}_b\boldsymbol{u})}\right|} \le \frac{\beta}{\alpha}. \tag{34}$$

This formula is not rigorous, but it provides a useful estimate of the condition number of the pre-conditioned system $\boldsymbol{A}_b^{-1}\boldsymbol{A}$, as will be illustrated by numerical examples. Since the frequency of the EM field and grid size are not involved in this estimate, the convergence of the chosen pre-conditioned iterative solver is expected to be invariant with respect to these parameters. However, the right-hand side of eq. (34) is essentially a measure of the conductivity contrast; thus, the solver will degrade on models with high-contrast anomalies. In the next section, we will develop a technique which significantly improves this result.

4 PRE-CONDITIONER BASED ON THE CONTRACTION OPERATOR

Estimate (34) is similar to that of the conventional IE method. That method is known to have difficulties for models with high conductivity contrast. In order to mitigate this problem the papers by Pankratov *et al.* (1995), Singer (1995), Zhdanov & Fang (1997), Hursan & Zhdanov (2002), Singer (2008) and Zhdanov (2009) developed a contraction integral equation operator and illustrated its robustness. In this section, we will derive an FD CO similar to one introduced in Hursan & Zhdanov (2002) and Zhdanov (2002) and will analyse the condition number of the respective problem.

Following the strategy of Zhdanov & Fang (1997), Hursan & Zhdanov (2002) and Zhdanov (2002), we introduce a modified FD Green's operator according to the following formula:

$$\boldsymbol{\mathcal{G}}_b^M = 2i\omega\mu_0\boldsymbol{\Sigma}_b^{\frac{1}{2}}\boldsymbol{A}_b^{-1}\boldsymbol{\Sigma}_b^{\frac{1}{2}} + \boldsymbol{I}. \tag{35}$$

Using this operator, eq. (23) can be written in an equivalent form as follows:

$$\widehat{\boldsymbol{e}}_a = \boldsymbol{\mathcal{G}}_b^M\boldsymbol{K}_2\boldsymbol{K}_1^{-1}\widehat{\boldsymbol{e}}_a + i\omega\mu_0\boldsymbol{\Sigma}_b^{\frac{1}{2}}\boldsymbol{A}_b^{-1}\boldsymbol{\Sigma}_a\boldsymbol{e}_b, \quad \widehat{\boldsymbol{e}}_a = \boldsymbol{K}_1\boldsymbol{e}_a, \tag{36}$$

where $\boldsymbol{K}_1$, $\boldsymbol{K}_2$ are diagonal matrices,

$$\boldsymbol{K}_1 = \frac{1}{2}(\boldsymbol{\Sigma} + \boldsymbol{\Sigma}_b)\boldsymbol{\Sigma}_b^{-\frac{1}{2}}, \quad \boldsymbol{K}_2 = \frac{1}{2}(\boldsymbol{\Sigma} - \boldsymbol{\Sigma}_b)\boldsymbol{\Sigma}_b^{-\frac{1}{2}}. \tag{37}$$

By introducing a new operator,

$$\boldsymbol{C} = \boldsymbol{\mathcal{G}}_b^M\boldsymbol{K}_2\boldsymbol{K}_1^{-1}, \tag{38}$$

we rewrite system (36) as follows:

$$\widehat{\boldsymbol{e}}_a = \boldsymbol{C}\widehat{\boldsymbol{e}}_a + i\omega\mu_0 \boldsymbol{\Sigma}_b^{\frac{1}{2}} \boldsymbol{A}_b^{-1} \boldsymbol{\Sigma}_a \boldsymbol{e}_b. \tag{39}$$

Finally, we arrive at the following pre-conditioned system of equations for the scaled anomalous electric field:

$$(\boldsymbol{I} - \boldsymbol{C})\widehat{\boldsymbol{e}}_a = i\omega\mu_0 \boldsymbol{\Sigma}_b^{\frac{1}{2}} \boldsymbol{A}_b^{-1} \boldsymbol{\Sigma}_a \boldsymbol{e}_b. \tag{40}$$

An important feature of the above equation is that operator $\boldsymbol{C}$ is a CO. Let us prove this by deducing an estimate of the norm of $\boldsymbol{C}$. We will also determine the condition number of $(\boldsymbol{I} - \boldsymbol{C})$, which is the system matrix of (40) and compare it with that of (23).

Note that Zhdanov & Fang (1997) and Zhdanov (2002, 2009) utilized the energy inequality for the anomalous field in order to prove a similar result for an integral equation operator. This inequality states that the energy flow of the anomalous EM field outside the anomalous domain is always non-negative (Zhdanov 2002, 2009). It was shown in Section 2 that the energy inequality takes the form of equality (11) when we complete Maxwell's equations with zero Dirichlet boundary conditions. In Appendix B, we have proved that FD approximations of the anomalous electric field and current, $\boldsymbol{e}_a$ and $\boldsymbol{j}_a$, satisfy a discrete energy equality,

$$\left\| \boldsymbol{\Sigma}_b^{\frac{1}{2}} \boldsymbol{e}_a \right\|^2 + \mathrm{Re}(\boldsymbol{e}_a, \boldsymbol{j}_a^*) = 0. \tag{41}$$

Applying some simple algebra, we can rewrite the equality as follows:

$$\left\| \boldsymbol{\Sigma}_b^{\frac{1}{2}} \boldsymbol{e}_a + \frac{1}{2} \boldsymbol{\Sigma}_b^{-\frac{1}{2}} \boldsymbol{j}_a \right\|^2 = \left\| \frac{1}{2} \boldsymbol{\Sigma}_b^{-\frac{1}{2}} \boldsymbol{j}_a \right\|^2. \tag{42}$$

Now, we substitute expression $\boldsymbol{e}_a = i\omega\mu_0 \boldsymbol{A}_b^{-1} \boldsymbol{j}_a$ into the last equality:

$$\left\| i\omega\mu_0 \boldsymbol{\Sigma}_b^{\frac{1}{2}} \boldsymbol{A}_b^{-1} \boldsymbol{j}_a + \frac{1}{2} \boldsymbol{\Sigma}_b^{-\frac{1}{2}} \boldsymbol{j}_a \right\|^2 = \left\| \frac{1}{2} \boldsymbol{\Sigma}_b^{-\frac{1}{2}} \boldsymbol{j}_a \right\|^2. \tag{43}$$

Introducing a new vector $\boldsymbol{v} = \frac{1}{2} \boldsymbol{\Sigma}_b^{-\frac{1}{2}} \boldsymbol{j}_a$, and taking into account eq. (35), we obtain:

$$\left\| 2i\omega\mu_0 \boldsymbol{\Sigma}_b^{\frac{1}{2}} \boldsymbol{A}_b^{-1} \boldsymbol{\Sigma}_b^{\frac{1}{2}} \boldsymbol{v} + \boldsymbol{v} \right\|^2 = \left\| \boldsymbol{\mathcal{G}}_b^M \boldsymbol{v} \right\|^2 = \|\boldsymbol{v}\|^2. \tag{44}$$

The last equality evidently proves that operator $\boldsymbol{\mathcal{G}}_b^M$ has its norm equal to one:

$$\left\| \boldsymbol{\mathcal{G}}_b^M \right\| = 1. \tag{45}$$

Equality (45) is the key fact needed to prove that $\boldsymbol{C}$ is a CO. Indeed, let us calculate its norm:

$$\|\boldsymbol{C}\| = \left\| \boldsymbol{\mathcal{G}}_b^M \boldsymbol{K}_2 \boldsymbol{K}_1^{-1} \right\| \le \left\| \boldsymbol{K}_2 \boldsymbol{K}_1^{-1} \right\|. \tag{46}$$

Thus it remains to estimate the norm of $\boldsymbol{K}_2 \boldsymbol{K}_1^{-1}$. This product is a diagonal matrix and its norm is equal to the largest entry. Substituting expressions for $\boldsymbol{K}_1$ and $\boldsymbol{K}_2$, we obtain

$$\left\| \boldsymbol{K}_2 \boldsymbol{K}_1^{-1} \right\| = \left\| \left(\boldsymbol{\Sigma}_b^{-1} \boldsymbol{\Sigma} - \boldsymbol{I} \right) \left(\boldsymbol{\Sigma}_b^{-1} \boldsymbol{\Sigma} + \boldsymbol{I} \right)^{-1} \right\|. \tag{47}$$

The non-zero entries of matrix $\boldsymbol{\Sigma}_b^{-1} \boldsymbol{\Sigma}$ belong to $[\alpha, \beta]$ due to inequality (25). Consequently, computation of the norm in (47) is equivalent to solution of the following optimization problem:

$$\left\| \boldsymbol{K}_2 \boldsymbol{K}_1^{-1} \right\| \le \max_{\xi \in [\alpha, \beta]} \frac{|\xi - 1|}{\xi + 1}. \tag{48}$$

The optimization problem on the right-hand side of inequality (48) can be easily solved, and we obtain

$$\left\| \boldsymbol{K}_2 \boldsymbol{K}_1^{-1} \right\| \le \max \left\{ \frac{1 - \alpha}{\alpha + 1}, \frac{\beta - 1}{\beta + 1} \right\}. \tag{49}$$

Since both of the fractions are less than one, we finally conclude

$$\|\boldsymbol{C}\| \le \left\| \boldsymbol{K}_2 \boldsymbol{K}_1^{-1} \right\| < 1. \tag{50}$$

This completes the proof that $\boldsymbol{C}$ is a CO.

Let us equivalently rewrite the later estimates:

$$\|\boldsymbol{C}\| \le 1 - 2 \min \left\{ \alpha/(\alpha + 1), \frac{1}{\beta + 1} \right\}. \tag{51}$$

The fundamental result is that $\boldsymbol{C}$ *is a CO for media of any contrast*, though its norm approaches 1 in the limiting cases.

The performance of iterative solvers depends on the condition number of the system matrix of equation (40). Let us find the condition number of $(\boldsymbol{I} - \boldsymbol{C})$. For any CO $\boldsymbol{C}$ the following estimate for the condition number could be derived (see Appendix C for the proof):

$$\mathrm{cond}(\boldsymbol{I} - \boldsymbol{C}) \le \frac{1 + \|\boldsymbol{C}\|}{1 - \|\boldsymbol{C}\|}. \tag{52}$$

Combining this formula with inequality (51) gives us

$$\mathrm{cond}(\boldsymbol{I} - \boldsymbol{C}) \le \max \left\{ \frac{1}{\alpha}, \beta \right\}. \tag{53}$$

In order to conclude our analysis of the two solvers, let us compare estimates (34) and (53) for the condition numbers of the two pre-conditioned systems. The two estimates provide a clear indication on how the two pre-conditioners are expected to perform.

We can see from these estimates that the convergence will be approximately the same for the models formed by conductive anomalies only ($\alpha = 1, \beta \ge 1$) as for those formed by resistive anomalies only ($\alpha \le 1, \beta = 1$). However, in a general case we may have both the conductive and resistive anomalies in the geoelectrical model ($\alpha < 1, \beta > 1$). In this situation, the solver based on the pre-conditioner formed by the CO will converge faster than with the pre-conditioner based on the background model. Note that the computational effort of the CO differs from the use of the background model Green's function in scaling by diagonal matrices $\boldsymbol{K}_2 \boldsymbol{K}_1^{-1}$, $\boldsymbol{\Sigma}_b^{\frac{1}{2}}$ and $2i\omega\mu_0 \boldsymbol{\Sigma}_b^{\frac{1}{2}}$, and two added vector additions from $\boldsymbol{I}$ terms in eqs (35) and (40). Since this effort is minor relative to that of computation $\boldsymbol{A}_b^{-1} \boldsymbol{u}$, we expect a better convergence of the FD solver based on the CO than of that based on the background model, and also a smaller CPU time. We will illustrate the performances of the developed methods in the next section.

5 NUMERICAL EXPERIMENTS

In this section, we present a numerical comparison of the two pre-conditioners discussed and analysed earlier. The first one is based on the discrete Green's function for the layered background model (i.e. eq. 23) and will be abbreviated as FD 1-D, while the second one is based on the designed CO (eq. 40) and will be abbreviated as CO. For an iterative solver we use BiCGStab (van der Vorst 1992; Saad 2003) for both pre-conditioners. This iterative solver performs two residual norm checks at each iteration. If the requested tolerance is achieved at the first check, the solver stops, and this corresponds to a fractional iteration number N_{it}. If the tolerance is achieved at the second check, this corresponds to a whole iteration number.

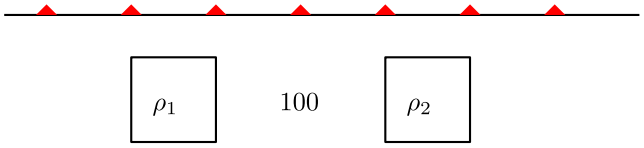

Figure 1. Two bodies having resistivities of $\rho_1 = 10$ and $\rho_2 = 1000$ Ωm, respectively, embedded in a half-space with a resistivity of 100 Ωm; the receivers are marked as triangles.

Table 1. Number of iterations and CPU time versus tolerance, ε, for the FD 1-D and CO pre-conditioners; $\rho_1 = 10$ and $\rho_2 = 1000$ Ωm.

	FD 1-D		CO	
ε	N_{it}	t	N_{it}	t
1e-4	12.0	108	6.5	62
1e-6	23.5	209	10.5	99
1e-8	38.5	340	14.5	128
1e-10	45.0	405	18.0	171
1e-12	56.5	503	21.0	195

5.1 Modelling magnetotelluric data

In order to test the discussed pre-conditioning algorithms, we considered a model adopted from Mehanee & Zhdanov (2002). The model is formed by two bodies $2 \times 2 \times 2$ km^3 each, having resistivities of $\rho_1 = 10$ and $\rho_2 = 1000$ Ωm respectively, and buried 1 km below the earth's surface (Fig. 1). The distance between the bodies is 4 km. The background is a half-space with a uniform resistivity of 100 Ωm. The model is excited by a 0.1 Hz incident plane wave. The receivers are placed every 250 m along a 12 km line which spans the bodies and is located symmetrically with respect to the inclusions, as shown in Fig. 1.

For this test, a non-uniform grid of $174 \times 160 \times 70$ cells was generated with the smallest cell size $250 \times 250 \times 250$ m^3; the discrete problem involved 5 744 364 unknowns. The computational domain spanned for 300 km in the horizontal directions and for 120 km in the vertical direction. A much smaller grid might have been used for this model. However, we used this fairly large grid for testing the effectiveness of the developed pre-conditioners. For each execution of the iterative solver, we recorded the number of iterations, N_{it}, and the CPU time in seconds, t, depending on the requested residual tolerance (Table 1). Fig. 2 illustrates the convergence process for the two pre-conditioners as well as for the Jacobi pre-conditioner.

Both the FD 1-D and CO pre-conditioned solvers were able to tackle this high-contrast problem, though the CO pre-conditioner was approximately twice more efficient than the FD 1-D pre-conditioner in this case. For the Jacobi pre-conditioner, 100 iterations were clearly not enough to reach a decent accuracy. The time needed for BiCGStab to perform 100 Jacobi pre-conditioned iteration was 160 s, implying that time spent on one iteration was 1.6 s. A similar parameter for a CO pre-conditioned iteration was 9.4 s. This means that a CO pre-conditioned iteration in this example took only about 6 times more than that of Jacobi. There is little difference in expense per iteration between the FD 1-D and the CO pre-conditioner as it was shown in the previous section. Fig. 3 presents plots of the real and imaginary parts of electric field E_x

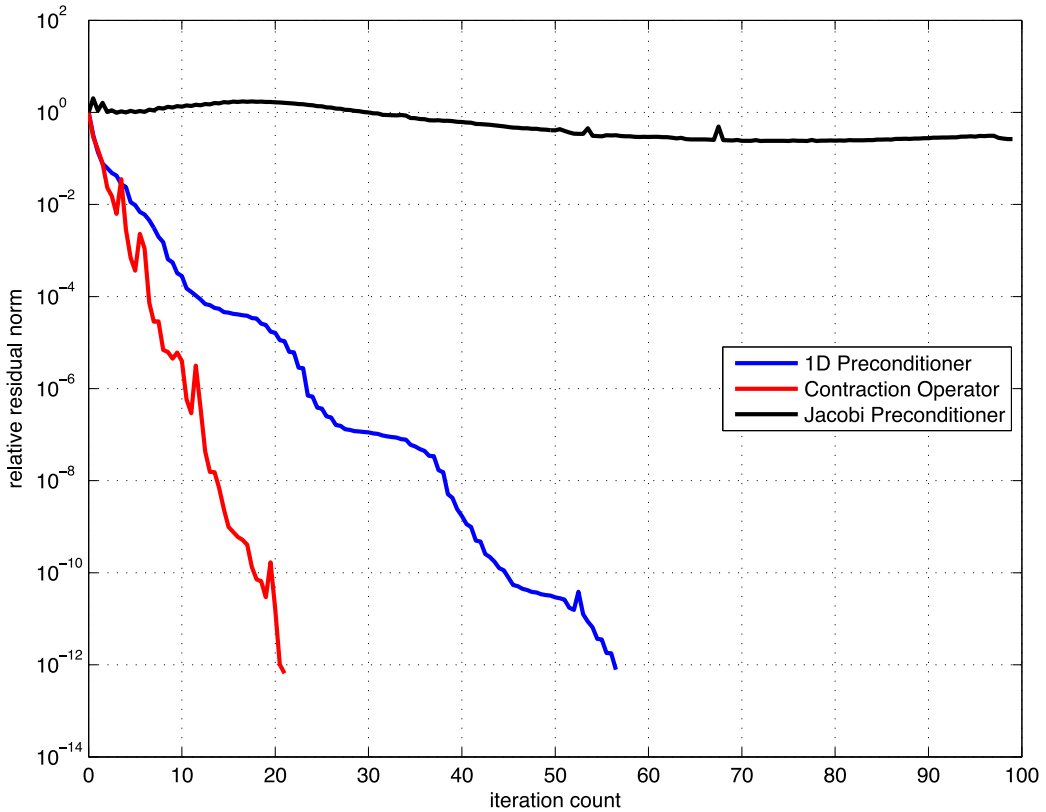

Figure 2. The plots of the l_2-norm of relative residuals versus iteration count for the FD 1-D pre-conditioner (blue line), contraction operator (red line) and Jacobi pre-conditioners (black line), respectively; $\rho_1 = 10$ and $\rho_2 = 1000$ Ωm.

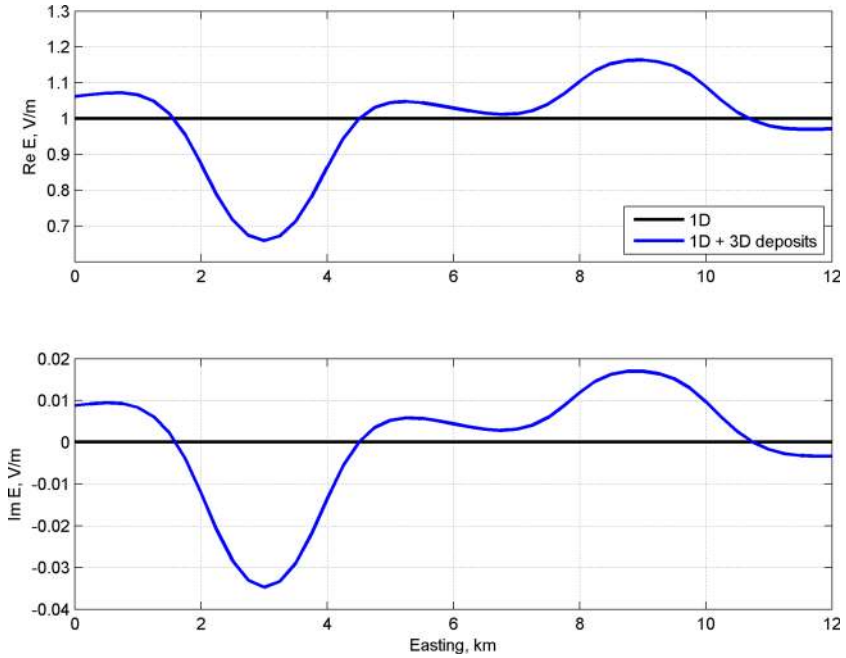

Figure 3. Real and imaginary parts of the electric field E_x along the profile; $\rho_1 = 10$ and $\rho_2 = 1000$ Ωm.

Table 2. Number of iterations and CPU time versus resistivity for the BiCGStab accuracy tolerance of $\varepsilon =$ 1e-6.

		FD 1-D		CO	
ρ_1	ρ_2	N_{it}	t	N_{it}	t
10	10	10.0	92	10.0	94
40	10	11.0	104	10.0	94
1000	1000	6.5	61	7.5	71
400	1000	8.0	74	9.0	86
10	1000	23.5	209	10.5	99

along the profile. We observed a decent sensitivity of the response to the anomalous bodies.

We also varied the resistivities of the two inclusions (Fig. 1), while keeping the background model ($\rho = 100$ Ωm), frequency (0.1 Hz), computational grid (174 × 160 × 70) and accuracy tolerance ($\varepsilon =$ 1e-6) fixed. We observed that the two solvers performed similarly when both inclusions were either resistive or conductive (Table 2). If there were both resistive and conductive inclusions, then the CO pre-conditioner was the fastest. This result was expected according to estimates (34) and (53).

5.2 Modelling marine CSEM data

In the next set of numerical experiments, we consider a complex geoelectric model of an offshore oil reservoir (Fig. 4). The model consists of a 200 m seawater layer with a resistivity of 0.25 Ωm, three sedimentary layers (4, 8 and 4 Ωm), a basement with a resistivity of 200 Ωm and a 100 Ωm reservoir. The reservoir has a complex shape and an approximate size 8 × 6 × 0.2 km^3. The model is partially based on the one tested in Li & Key (2007).

The EM field at a frequency of 0.25 Hz was generated by a horizontal electric dipole source located at (0, 0, 10) m. An array of inline electric receivers was located at the depth of the source.

In this example, we generated a non-uniform 202 × 182 × 97 grid with the smallest cell size 125 × 125 × 50 m^3; thus, the discrete problem involved nearly 10 million unknowns. We sampled the model onto this grid as illustrated in Fig. 5.

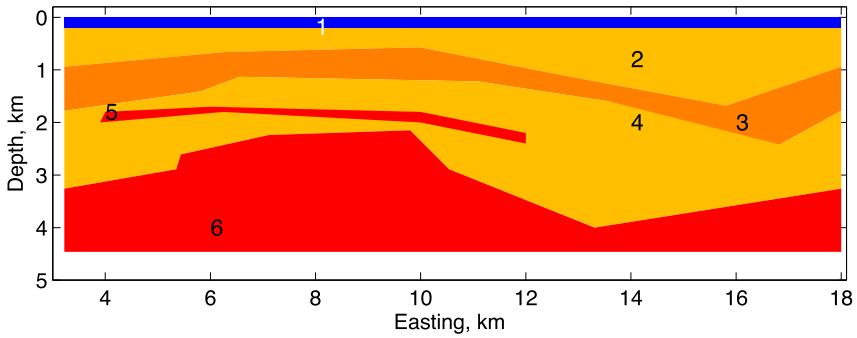

Figure 4. Vertical cross-section of the offshore oilfield model: (1) seawater layer, (2) 4 Ωm sedimentary layer, (3) 8 Ωm sedimentary layer, (4) 4 Ωm sedimentary layer, (5) 100 Ωm hydrocarbon deposit, (6) 200 Ωm basement.

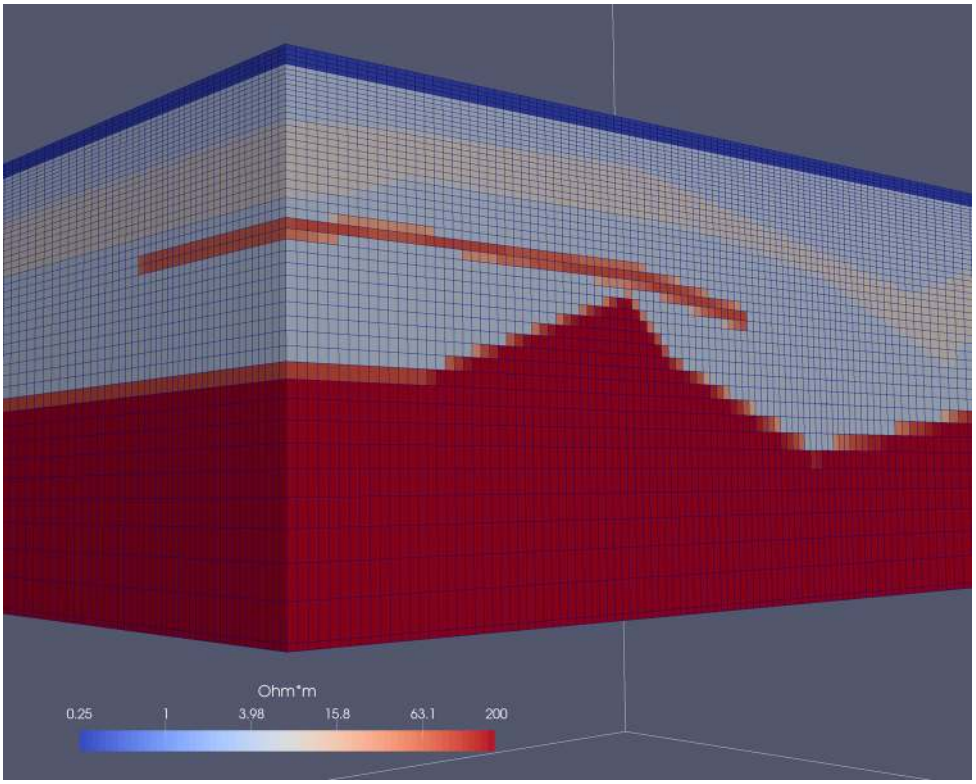

Figure 5. Volume view of the offshore oilfield model sampled onto computational grid cells.

Table 3. Iteration count and CPU time in modelling of the CSEM data for the offshore oilfield model.

FD 1-D		CO	
N_{it}	t	N_{it}	t
148.0	3407	31.5	733

As in the previous examples, we tested the BiCGStab iterative solver leveraged with the FD 1-D and CO pre-conditioners. The iteration count and execution time are shown in Table 3. We observed that the use of the CO pre-conditioner gave us a speed-up of almost five times. This result can be explained as follows. Due to variations of the basement depth, the horizontal contrast coefficients (24) are equal to $\alpha = 1/50$ and $\beta = 50$. Substitution of these values into condition number estimates (34) and (53) suggests that the condition number for the CO system is 50 times smaller, implying $\sqrt{50} \approx 7$ times faster convergence. This is what we roughly observed in the numerical tests.

We finalized this test with an illustration of the simulated responses for the oilfield model. Fig. 6 shows the response for the models with and without a hydrocarbon deposit. We observed a sensitivity of about 19 per cent for the amplitude and about 12° for the phase of the electric field response.

6 CONCLUSIONS

In this paper, we have introduced a novel pre-conditioner for the FD system of EM equations. This pre-conditioner represents an FD analogue of the well-known pre-conditioner of the system of the EM integral equations based on the CO. The new pre-conditioner can be easily constructed using the known conductivity distribution in the model. This pre-conditioner makes it possible to speed up the convergence of the iterative solvers of the FD equations significantly. We have also demonstrated that this pre-conditioner provides a better condition number for the system of FD equations than the one based on the discrete Green's function for the background EM model only. This result was illustrated with numerical examples for different geophysical applications. Beyond this, both of the pre-conditioners are very memory-economical.

Future research will be aimed at extending the developed algorithms for the cases of anisotropic geoelectrical models, which will be the subject of another paper.

ACKNOWLEDGEMENTS

The authors acknowledge the MIPT, University of Utah's Consortium for Electromagnetic Modeling and Inversion (CEMI) and TechnoImaging, for support of this research and permission to publish. We also thank Mikhail Malovichko for assistance in preparation of the geoelectrical model of the offshore hydrocarbon reservoir.

The authors appreciate the constructive remarks by the editor and anonymous reviewers, which helped to improve the manuscript.

This research was supported by the Russian Science Foundation, project No. 16-11-10188.

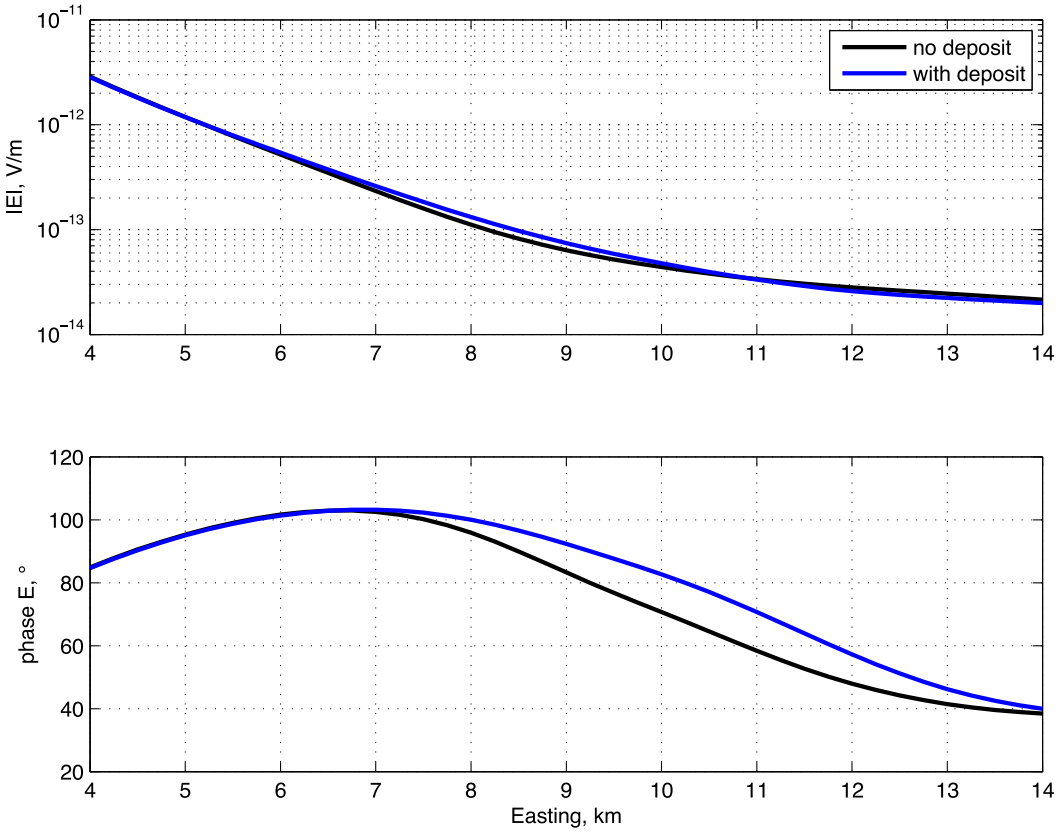

Figure 6. Sensitivity of the electric field data to the hydrocarbon deposit.

REFERENCES

Arnold, D.N., Falk, R.S. & Winther, R., 2000. Multigrid in H(div) and H(curl), *Numer. Math.,* **85**(2), 197–217.

Avdeev, D.B., 2005. Three-dimensional electromagnetic modelling and inversion from theory to application, *Surv. Geophys.,* **26**(6), 767–799.

Cai, H., Xiong, B., Han, M. & Zhdanov, M., 2014. 3D controlled-source electromagnetic modeling in anisotropic medium using edge-based finite element method, *Comput. Geosci.,* **73**(0), 164–176.

Commer, M. & Newman, G., 2004. A parallel finite-difference approach for 3D transient electromagnetic modeling with galvanic sources, *Geophysics,* **69**(5), 1192–1202.

Commer, M. & Newman, G.A., 2008. New advances in three-dimensional controlled-source electromagnetic inversion, *Geophys. J. Int.,* **172**(2), 513–535.

da Silva, N.V., Morgan, J.V., MacGregor, L. & Warner, M., 2012. A finite element multifrontal method for 3D CSEM modeling in the frequency domain, *Geophysics,* **77**(2), E101–E115.

Dmitriev, V.I., 1969. Electromagnetic fields in inhomogeneous media (in Russian), in *Proceeding of the Computational Center,* Moscow State University.

Druskin, V. & Knizhnerman, L., 1994. Spectral approach to solving three-dimensional Maxwell's diffusion equations in the time and frequency domains, *Radio Sci.,* **29**(4), 937–953.

Grayver, A.V. & Bürg, M., 2014. Robust and scalable 3-D geo-electromagnetic modelling approach using the finite element method, *Geophys. J. Int.,* **198**(1), 110–125.

Grayver, A.V., Streich, R. & Ritter, O., 2013. Three-dimensional parallel distributed inversion of CSEM data using a direct forward solver, *Geophys. J. Int.,* **193**(3), 1432–1446.

Hohmann, G.W., 1975. Three-dimensional induced polarization and electromagnetic modeling, *Geophysics,* **40**(2), 309–324.

Hursan, G. & Zhdanov, M.S., 2002. Contraction integral equation method in three-dimensional electromagnetic modeling, *Radio Sci.,* **37**(6), doi:10.1029/2001RS002513.

Jaysaval, P., Shantsev, D. & de la Kethulle de Ryhove, S., 2014. Fast multimodel finite-difference controlled-source electromagnetic simulations based on a Schur complement approach, *Geophysics,* **79**(6), E315–E327.

Koldan, J., Puzyrev, V., de la Puente, J., Houzeaux, G. & Cela, J.M., 2014. Algebraic multigrid pre-conditioning within parallel finite-element solvers for 3-D electromagnetic modelling problems in geophysics, *Geophys. J. Int.,* **197**(3), 1442–1458.

Li, Y. & Key, K., 2007. 2D Marine controlled-source electromagnetic modeling: Part 1—An adaptive finite-element algorithm, *Geophysics,* **72**(2), WA51–WA62.

Maaø, F., 2007. Fast finite-difference time-domain modeling for marine-subsurface electromagnetic problems, *Geophysics,* **72**(2), A19–A23.

Mackie, R.L., Smith, J.T. & Madden, T.R., 1994. Three-dimensional electromagnetic modeling using finite difference equations: the magnetotelluric example, *Radio Sci.,* **29**(4), 923–935.

Marinenko, A., Epov, M. & Shurina, E., 2009. Modeling electromagnetic field in shelf areas, *Russ. Geol. Geophys.,* **50**(5), 475–484.

Martikainen, J., Rossi, T., Rogovin, K. & Toivanen, J., 2003. Fast direct solver for a time-harmonic electromagnetic problem with an application, in *Mathematical and Numerical Aspects of Wave Propagation, WAVES 2003,* pp. 675–680, eds Cohen, G., Joly, P., Heikkola, E. & Neittaanmäki, P., Springer.

Mehanee, S. & Zhdanov, M., 2002. Two-dimensional magnetotelluric inversion of blocky geoelectrical structures, *J. geophys. Res.,* **107**(B4), EPM 2-1–EPM 2-11.

Monk, P. & Süli, E., 1994. A convergence analysis of Yee's scheme on nonuniform grids, *SIAM J. Numer. Anal.,* **31**(2), 393–412.

Moskow, S., Druskin, V., Habashy, T., Lee, P. & Davydycheva, S., 1999. A finite difference scheme for elliptic equations with rough coefficients

using a cartesian grid nonconforming to interfaces, *SIAM J. Numer. Anal.,* **36**(2), 442–464.
Mulder, W.A., 2007. A robust solver for CSEM modelling on stretched grids, in *69th EAGE Conference and Exhibition,* EAGE.
Mulder, W.A., 2008. Geophysical modelling of 3D electromagnetic diffusion with multigrid, *Comput. Vis. Sci.,* **11**(3), 129–138.
Newman, G.A. & Alumbaugh, D.L., 2002. Three-dimensional induction logging problems, Part 2: A finite-difference solution, *Geophysics,* **67**(2), 484–491.
Newman, G.A., Hohmann, G.W. & Anderson, W.L., 1986. Transient electromagnetic response of a three-dimensional body in a layered earth, *Geophysics,* **51**(8), 1608–1627.
Pankratov, O.V., Avdeyev, D.B. & Kuvshinov, A.V., 1995. Electromagnetic field scattering in a heterogeneous earth: a solution to the forward problem, *Phys. Solid Earth (Engl. Ed.),* **31**(3), 201–209.
Puzyrev, V. & Cela, J.M., 2015. A review of block Krylov subspace methods for multisource electromagnetic modelling, *Geophys. J. Int.,* **202**(2), 1241–1252.
Quarteroni, A. & Valli, A., 2008. *Numerical Approximation of Partial Differential Equations,* Springer Series in Computational Mathematics, Springer.
Ren, Z., Kalscheuer, T., Greenhalgh, S. & Maurer, H., 2014. A finite-element-based domain-decomposition approach for plane wave 3D electromagnetic modeling, *Geophysics,* **79**(6), E255–E268.
Saad, Y., 2003. *Iterative Methods for Sparse Linear Systems,* 2nd edn, SIAM.
Schuhmann, R. & Weiland, T., 2001. Conservation of discrete energy and related laws in the finite integration technique, *Prog. Electromagn. Res.,* **32,** 301–316.
Singer, B.S., 1995. Method for solution of Maxwell's equations in non-uniform media, *Geophys. J. Int.,* **120**(3), 590–598.
Singer, B.S., 2008. Electromagnetic integral equation approach based on contraction operator and solution optimization in Krylov subspace, *Geophys. J. Int.,* **175**(3), 857–884.
Singer, B.S., Mezzatesta, A. & Wang, T., 2003. Integral equation approach based on contraction operators and Krylov subspace optimization, *ASEG Extended Abstracts,* **2003**(1), 1–14.
Smith, J.T., 1996. Conservative modeling of 3-D electromagnetic fields, Part II: Biconjugate gradient solution and an accelerator, *Geophysics,* **61**(5), 1319–1324.
Streich, R., 2009. 3D finite-difference frequency-domain modeling of controlled-source electromagnetic data: direct solution and optimization for high accuracy, *Geophysics,* **74**(5), F95–F105.
Tikhonov, A. & Samarskii, A., 1999. *Uravneniya matematicheskoi fisiki,* Moscow University Publications.
Um, E.S., Commer, M. & Newman, G.A., 2013. Efficient pre-conditioned iterative solution strategies for the electromagnetic diffusion in the earth: finite-element frequency-domain approach, *Geophys. J. Int.,* **193**(3), 1460–1473.
Van Bladel, J., 2007. *Electromagnetic Fields,* IEEE Press Series on Electromagnetic Wave Theory, John Wiley & Sons.
van der Vorst, H.A., 1992. Bi-CGSTAB: a fast and smoothly converging variant of Bi-CG for the solution of nonsymmetric linear systems, *SIAM J. Sci. Stat. Comput.,* **13**(2), 631–644.
Weidelt, P., 1975. Electromagnetic induction in three-dimensional structures, *J. Geophys,* **41,** 85–109.
Weidelt, P., 2000. Numerical modeling of transient-electromagnetic fields in three-dimensional conductors: a comparative study, Elektromagnetische Tiefenforschung, Kolloquiumsband zur Tagung in Altenberg, 216–230.
Weiss, C.J. & Constable, S., 2006. Mapping thin resistors and hydrocarbons with marine EM methods, Part II – Modeling and analysis in 3D, *Geophysics,* **71**(6), G321–G332.
Weiss, C.J. & Newman, G.A., 2002. Electromagnetic induction in a fully 3-D anisotropic earth, *Geophysics,* **67**(4), 1104–1114.
Yavich, N. & Scholl, C., 2012. Advances in multigrid solution of 3D forward MCSEM problem, in *5th EAGE St. Petersburg International Conference and Exhibition on Geosciences,* EAGE.
Yee, K., 1966. Numerical solution of initial boundary value problems involving Maxwell's equations in isotropic media, *IEEE Trans. Antennas Propag.,* **14**(3), 302–307.
Zaslavsky, M., Druskin, V., Davydycheva, S., Knizhnerman, L., Abubakar, A. & Habashy, T., 2011. Hybrid finite-difference integral equation solver for 3D frequency domain anisotropic electromagnetic problems, *Geophysics,* **76**(2), F123–F137.
Zhdanov, M., 2002. *Geophysical Inverse Theory and Regularization Problems,* vol. 36, Elsevier.
Zhdanov, M., 2009. *Geophysical Electromagnetic Theory and Methods,* Methods in Geochemistry and Geophysics, Elsevier Science.
Zhdanov, M.S. & Fang, S., 1997. Quasi-linear series in three-dimensional electromagnetic modeling, *Radio Sci.,* **32**(6), 2167–2188.

APPENDIX A: DISCRETIZATION OF THE ELECTRIC FIELD EQUATIONS USING A STAGGERED GRID

In this appendix, we introduce discrete unknowns to approximate the electric field on a staggered grid. To simplify the notations, we will limit our discussion to eq. (1), although discretization of eq. (5) could be obtained in a similar way.

We assume that some non-uniform Cartesian grid covering computational domain V is given. An actual algorithm to generate such a grid is based on the notion of skin depth and is not discussed in this note. Let us denote grid lines as

$$\{x_i\}, \quad i = 1..N_x + 1,$$
$$\{y_j\}, \quad j = 1..N_y + 1,$$
$$\{z_k\}, \quad k = 1..N_z + 1, \tag{A1}$$

where N_x, N_y and N_z are grid cell numbers in the respective directions. We also need staggered grid lines,

$$x_{i+\frac{1}{2}} = \frac{1}{2}(x_{i+1} + x_i), \quad i = 1..N_x,$$
$$y_{j+\frac{1}{2}} = \frac{1}{2}(y_{j+1} + y_j), \quad j = 1..N_y,$$
$$z_{k+\frac{1}{2}} = \frac{1}{2}(z_{k+1} + z_k), \quad k = 1..N_z. \tag{A2}$$

Finally, we need volumes associated with each internal edge of the grid:

$$V_{i+\frac{1}{2}\,j\,k} = [x_i, x_{i+1}] \times \left[y_{j-\frac{1}{2}}, y_{j+\frac{1}{2}}\right] \times \left[z_{k-\frac{1}{2}}, z_{k+\frac{1}{2}}\right],$$
$$V_{i\,j+\frac{1}{2}\,k} = \left[x_{i-\frac{1}{2}}, x_{i+\frac{1}{2}}\right] \times [y_j, y_{j+1}] \times \left[z_{k-\frac{1}{2}}, z_{k+\frac{1}{2}}\right],$$
$$V_{i\,j\,k+\frac{1}{2}} = \left[x_{i-\frac{1}{2}}, x_{i+\frac{1}{2}}\right] \times \left[y_{j-\frac{1}{2}}, y_{j+\frac{1}{2}}\right] \times [z_k, z_{k+1}]. \tag{A3}$$

The FD method approximates (Yee 1966; Monk & Süli 1994) the unknown electric field $E = (E_x, E_y, E_z)$ with a finite set of discrete values $\{E_{i+\frac{1}{2}\,j\,k}, E_{i\,j+\frac{1}{2}\,k}, E_{i\,j\,k+\frac{1}{2}}\}$,

$$E_{i+\frac{1}{2}\,j\,k} \approx E_x\left(x_{i+\frac{1}{2}}, y_j, z_k\right),$$
$$E_{i\,j+\frac{1}{2}\,k} \approx E_y\left(x_i, y_{j+\frac{1}{2}}, z_k\right),$$
$$E_{i\,j\,k+\frac{1}{2}} \approx E_z\left(x_i, y_j, z_{k+\frac{1}{2}}\right). \tag{A4}$$

Each discrete value is associated with the respective edge of the FD grid, Fig. A1.

In the derivations, we use $\sigma_{i+\frac{1}{2}\,j\,k}$, $\sigma_{i\,j+\frac{1}{2}\,k}$, $\sigma_{i\,j\,k+\frac{1}{2}}$, which are edge-sampled conductivities. For example, in the framework of the so-called integro-interpolation scheme for coefficients averaging

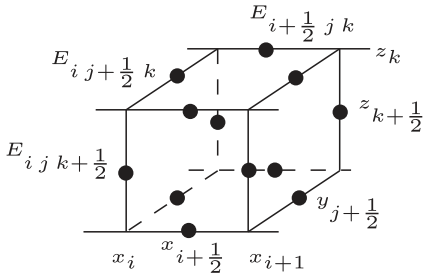

Figure A1. Finite-difference cell.

(Moskow *et al.* 1999; Tikhonov & Samarskii 1999; Commer & Newman 2008), we have

$$\sigma_{i+\frac{1}{2}\,j\,k} = \frac{x_{i+1}-x_i}{\left(y_{j+\frac{1}{2}}-y_{j-\frac{1}{2}}\right)\left(z_{k+\frac{1}{2}}-z_{k-\frac{1}{2}}\right)} \times \left(\int_{x_i}^{x_{i+1}}\left(\int_{z_{k-\frac{1}{2}}}^{z_{k+\frac{1}{2}}}\int_{y_{j-\frac{1}{2}}}^{y_{j+\frac{1}{2}}}\sigma(x,y,z)\mathrm{d}y\mathrm{d}z\right)^{-1}\mathrm{d}x\right)^{-1}. \quad \text{(A5)}$$

Note that there exist more advanced material-averaging schemes (Moskow *et al.* 1999). However, in this paper we use a standard integro-interpolation scheme for simplicity.

Finally, we also use the sampled source,

$$J_{i+\frac{1}{2}\,j\,k} = \frac{1}{\left|V_{i+\frac{1}{2}\,j\,k}\right|}\int_{V_{i+\frac{1}{2}\,j\,k}} J_x(x,y,z)\mathrm{d}V, \quad \text{(A6)}$$

and similarly $J_{i\,j+\frac{1}{2}\,k}$ and $J_{i\,j\,k+\frac{1}{2}}$ are defined.

The actual discrete equations can be found, for example, in Weiss & Newman (2002). Fig. A2 illustrates the obtained stencils of the equations. The presented discretization is known to have locally first order accuracy, while globally it has second-order accuracy (Monk & Süli 1994). In practice, this implies that we prefer equidistant grids near the receiver locations.

Let us form the unknown vector $\boldsymbol{e}$ of the discrete electric fields $\{E_{i+\frac{1}{2}\,j\,k}, E_{i\,j+\frac{1}{2}\,k}, E_{i\,j\,k+\frac{1}{2}}\}$ introduced above. First we enumerate the electric fields assigned to the edges parallel to the x axis, then those parallel to y, and finally those parallel to z. Within each set of edges, we assume the lexicographic $x-y-z$ order. If we denote as n the total number of internal edges, then the FD electric field $\boldsymbol{e}$ belongs to the complex linear space $\mathbb{C}^n$,

$$n = N_x(N_y-1)(N_z-1) + (N_x-1)N_y(N_z-1) + (N_x-1)(N_y-1)N_z. \quad \text{(A7)}$$

Using the same enumeration, we form a right-hand vector $\boldsymbol{j}\in\mathbb{C}^n$ of $\{J_{i+\frac{1}{2}\,j\,k}, J_{i\,j+\frac{1}{2}\,k}, J_{i\,j\,k+\frac{1}{2}}\}$. Now we can write the FD discretization of eq. (1) in a matrix form:

$$\boldsymbol{A}\boldsymbol{e} = i\omega\mu_0\boldsymbol{j}. \quad \text{(A8)}$$

Some properties of $\boldsymbol{A}$ were discussed in Section 3.

APPENDIX B: DISCRETE ENERGY EQUALITY

In this appendix, we introduce a discrete energy equality, which is used in determining the properties of the FD CO. The derivation of the discrete equation is similar to that of the continuous equation (11), however, we present this derivation for completeness. This derivation relies on semi-positiveness of FD curl-curl matrix $\boldsymbol{R}$ (see eq. 29).

Let us substitute eq. (15) into eq. (16),

$$\boldsymbol{R}\boldsymbol{e}_a - i\omega\mu_0\boldsymbol{\Sigma}_b\boldsymbol{e}_a = i\omega\mu_0\boldsymbol{j}_a. \quad \text{(B1)}$$

Using the pseudo-scalar product (26), let us multiply this equation by $\boldsymbol{e}_a^*$:

$$(\boldsymbol{e}_a^*, \boldsymbol{R}\boldsymbol{e}_a) - i\omega\mu_0(\boldsymbol{e}_a^*, \boldsymbol{\Sigma}_b\boldsymbol{e}_a) = i\omega\mu_0(\boldsymbol{e}_a^*, \boldsymbol{j}_a). \quad \text{(B2)}$$

Dividing by $i\omega\mu_0$, taking the real part, and noting semi-positiveness of $\boldsymbol{R}$ (29), we obtain:

$$(\boldsymbol{e}_a^*, \boldsymbol{\Sigma}_b\boldsymbol{e}_a) + \mathrm{Re}(\boldsymbol{e}_a^*, \boldsymbol{j}_a) = 0. \quad \text{(B3)}$$

The last equality can be rewritten as follows using the definition of the norm (27),

$$\left\|\boldsymbol{\Sigma}_b^{\frac{1}{2}}\boldsymbol{e}_a\right\|^2 + \mathrm{Re}(\boldsymbol{e}_a, \boldsymbol{j}_a^*) = 0. \quad \text{(B4)}$$

This completes the proof of the discrete energy equality. As for its continuous version (11), it states that the energy introduced through the anomalous currents is equal the radiated Joule heating.

APPENDIX C: CONDITION NUMBER OF AN EQUATION SYSTEM INVOLVING A CONTRACTION OPERATOR

We consider eq. (40) written in a compact form as follows:

$$(\boldsymbol{I}-\boldsymbol{C})\boldsymbol{u} = \boldsymbol{f}, \quad \text{(C1)}$$

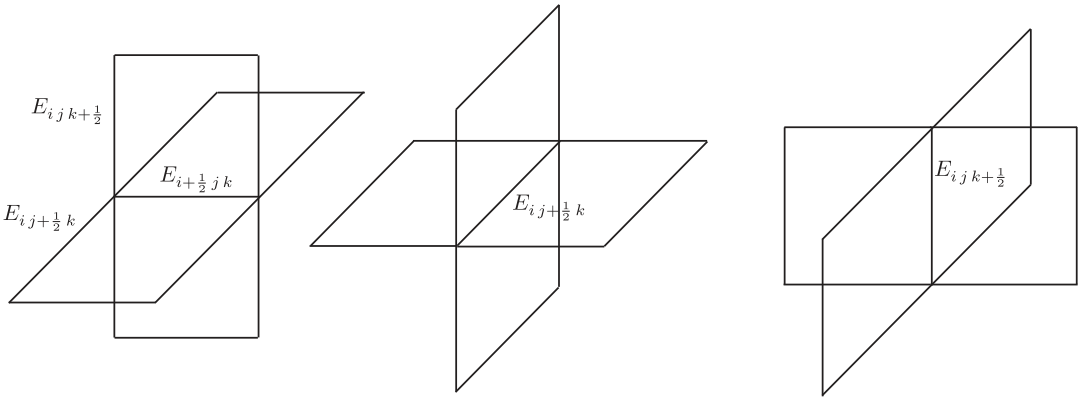

Figure A2. Discretization stencils for eq. (1).

with $\boldsymbol{C}$ being a CO, that is, $\|\boldsymbol{C}\| < 1$, $\boldsymbol{I}$ is the identity matrix and $\boldsymbol{f} = i\omega\mu_0 \boldsymbol{\Sigma}_b^{\frac{1}{2}} \boldsymbol{A}_b^{-1} \boldsymbol{\Sigma}_a \boldsymbol{e}_b$ is a known complex vector. In this appendix, we estimate the condition number of this system, given by the following formula:

$$\mathrm{cond}(\boldsymbol{I} - \boldsymbol{C}) = \|\boldsymbol{I} - \boldsymbol{C}\| \|(\boldsymbol{I} - \boldsymbol{C})^{-1}\|. \tag{C2}$$

Using basic properties of the norm, we find

$$\|\boldsymbol{I} - \boldsymbol{C}\| \leq 1 + \|\boldsymbol{C}\|. \tag{C3}$$

To estimate the second multiplier in eq. (C2), we use Neumann series expansion:

$$\|(\boldsymbol{I} - \boldsymbol{C})^{-1}\| = \left\| \sum_{k=0}^{\infty} \boldsymbol{C}^k \right\| \leq \sum_{k=0}^{\infty} \|\boldsymbol{C}\|^k = \frac{1}{1 - \|\boldsymbol{C}\|}. \tag{C4}$$

Combining these inequalities, we finally determine the condition number of this system:

$$\mathrm{cond}(\boldsymbol{I} - \boldsymbol{C}) \leq \frac{1 + \|\boldsymbol{C}\|}{1 - \|\boldsymbol{C}\|}. \tag{C5}$$